JACS
JOURNAL OF THE AMERICAN CHEMICAL SOCIETY

Article

pubs.acs.org/JACS

Noble-Metal-Free Fe–N/C Catalyst for Highly Efficient Oxygen Reduction Reaction under Both Alkaline and Acidic Conditions

Ling Lin, Qing Zhu, and An-Wu Xu*

Division of Nanomaterials and Chemistry, Hefei National Laboratory for Physical Sciences at Microscale, University of Science and Technology of China, Hefei 230026, China

Supporting Information

ABSTRACT: In this work, we report the synthesis and assessment of a new non-precious-metal oxygen reduction reaction (ORR) catalyst from pyrolysis of an iron-coordinated complex which manifests superior activity in both alkaline and acidic media. 11,11′-bis(dipyrido[3,2-*a*:2′,3′-*c*]phenazinyl) (bidppz) was selected as a ligand for the formation of a nitrogen-rich iron-coordinated coordination polymer (Fe–bidppz) which forms a self-supporting catalyst containing high densities of nitrogen and iron doping by pyrolysis. The catalyst pyrolyzed at 800 °C (Fe–N/C-800) shows the highest ORR activity with onset and half-wave potentials of 923 and 809 mV in 0.1 M KOH, respectively, which are comparable to those of Pt/C (half-wave potential 818 mV vs RHE) at the same catalyst loading. Besides, the Fe–N/C-800 catalyst has an excellent ORR activity with onset and half-wave potentials only 38 and 59 mV less than those of the Pt/C catalyst in 0.1 M $HClO_4$. The optimal Fe–N/C-800 catalyst displays much greater durability and tolerance of methanol than Pt/C. We propose that the Fe–N/C-800 catalyst has a considerably high density of surface active sites because Fe–N/C-800 possesses excellent ORR activity while its specific surface area is not so high. Electrochemical measurements show that the Fe–N/C-800 catalyst in KOH and $HClO_4$ follows the effective four-electron-transfer pathway.

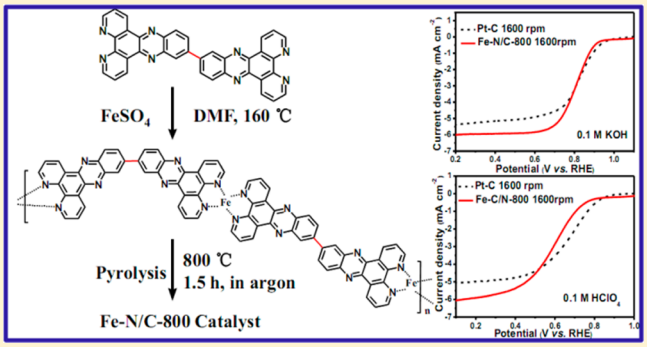

INTRODUCTION

The oxygen reduction reaction (ORR) at the cathode is an important process in proton exchange membrane fuel cells (PEMFCs) and is a major limiting factor of energy-conversion efficiency in PEMFCs. Platinum and its alloys are the most effective and commercially available ORR catalysts in PEMFCs under the harsh acidic conditions.[1] However, the high cost and low abundance of the precious metals limit the wide application of PEMFCs. Consequently, a range of alternative non-precious-metal catalysts (NPMCs) have been developed to facilitate the ORR on electrodes in the past few decades, including metal-free nitrogen-doped carbon (N-doped C),[2−4] non-precious-metal oxides and carbides,[5,6] transition-metal-coordinating macrocyclic compounds,[7,8] and transition-metal-coordinating nitrogen-doped carbon catalysts (M–N/C).[9−11] Up to now, only the M–N/C catalysts with Fe and/or Co have been found to possess good activity and durability in an acidic medium.[10,12,13] Unfortunately, M–N/C catalysts still suffer from inactivation because of the protonization of N atoms and anion bonding to active sites.[14,15]

The use of M–N/C catalysts as NPMCs began in the 1960s due to the discovery of cobalt phthalocyanine with ORR activity in alkaline conditions,[16] followed by the investigation of pyrolysis of these transition-metal macrocycles to improve their ORR catalytic activity and stability, especially in acidic electrolytes.[17−19] In recent years, in addition to macrocycles, a series of low-cost nitrogen precursors such as polyacrylonitrile (PAN), polypyrrole (PPy), polyaniline (PANI), ethylenediamine (EN), and cyanamide (CA) were utilized in the preparation of M–N/C catalysts by doping carbon supports with these metal-coordinating polymers.[20−24] Although pyrolyzed M–N/C catalysts have high activity and stability, the exact nature of the active sites of M–N/C in acidic media is still under debate whether the transition metal acts as the activity center or whether the transition metal only facilitates the formation of active nitrogen–carbon functional sites.[25−28] Nevertheless, plenty of studies have shown that the choice of nitrogen precursors, transition-metal species, carbon support morphology, and pyrolysis temperature greatly influence the activity of the catalyst.[13,22] Hence, recent research on M–N/C ORR catalysts has mainly focused on the above several aspects.

In this study, we have developed an iron-coordinated nitrogen-doped carbon catalyst (Fe–N/C) using a nitrogen-rich ligand, 11,11′-bis(dipyrido[3,2-*a*:2′,3′-*c*]phenazinyl) (bidppz) as the nitrogen-rich precursor, the structure of which is two dipyrido[3,2-*a*:2′,3′-*c*]phenazine (dppz) moieties linked by a C–C single bond. When coordinated with iron, bidppz molecules form a coordination polymer (Fe–bidppz) consisting of alternating chains of ligand and iron which hinders

Received: May 11, 2014
Published: July 24, 2014

   dx.doi.org/10.1021/ja504696r | *J. Am. Chem. Soc.* 2014, 136, 11027−11033

the agglomeration of iron species during the subsequent heat treatment. Furthermore, the C−C single bond connecting two dppz groups is readily rotatable, which results in numerous configurations of bidppz and a network structure of Fe−bidppz. Unlike the liner polymers previously used for M−N/C catalysts, this network complex can be utilized as a self-supporting catalyst excluding the use of a carbon support.[9,20−22,29] The nearly 20 wt % concentration of highly thermally stable pyridinic nitrogen in bidppz allows for a high degree of Fe−N coordination at high pyrolysis temperatures. We demonstrate that our catalyst (Fe−N/C-800) prepared by heating the Fe−bidppz precursor to 800 °C exhibits superior ORR catalytic activity, long-term stability, and higher methanol tolerance than the 20 wt % Pt/C (hereafter "Pt/C") catalyst in both alkaline and acidic media at a catalyst loading of 0.1 mg cm^{-2}. Overall, this self-supporting Fe−N/C-800 catalyst is a potential candidate as a highly efficient, stable, and low-cost ORR catalyst.

RESULTS AND DISCUSSION

Figure 1 depicts the chemical structure of bidppz, the synthetic process of the Fe−N/C-800 catalyst, and the corresponding

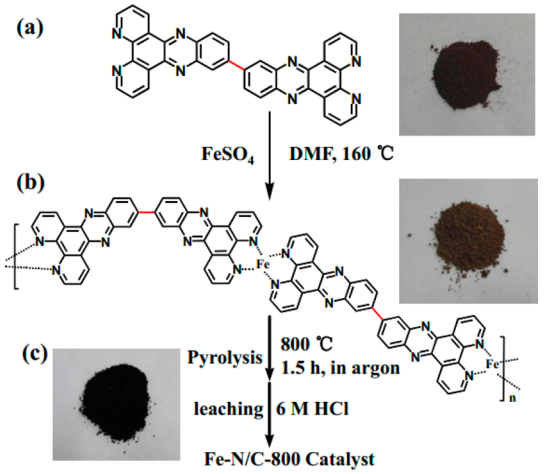

Figure 1. Schematic illustration of the synthetic process of the Fe−N/C-800 catalyst: (a) chemical structure and photograph of bidppz, (b) chemical structure and photograph of the corresponding Fe−bidppz precursor, (c) photograph of the obtained Fe−N/C-800 catalyst.

photographs. The rotatable C−C single bond linking two dppz moieties in the bidppz molecule (Figure 1a) is marked in red; the rotation of the C−C single bond produces different configurations of bidppz. A simple solvothermal in situ metal/ligand reaction was used to synthesize the Fe−bidppz precursor. The solvothermal technique is able to not only overcome the difficulties resulting from different solubilities of organic and inorganic precursors, but also produce products that are inaccessible or not easily obtainable by conventional methods.[30,31] The structure of the obtained Fe−bidppz complex is shown in Figure 1b, in which two different planar configurations of bidppz are displayed. Nevertheless, other nonplanar configurations may also appear in the Fe−bidppz complex, which leads to a network coordination polymer. This coordination polymer structure is effective at separating one iron site from another and preventing the iron sites from agglomeration during heat treatment, facilitating the formation of well-dispersed active sites. In addition, the quintuple aromatic ring structures in bidppz are highly thermally stable,[32] promoting graphitization during carbonization at a high temperature,[33,34] which is favorable for the high activity of the catalyst. The Fe−bidppz precursor was pyrolyzed in argon at 800 °C for 1.5 h, and the product was ultrasonically leached in 6 M hydrochloric acid (HCl) solution to obtain the Fe−N/C-800 self-supporting catalysts (Figure 1c). The aim of the leaching process is to remove the inactive iron particles and other iron species produced from agglomeration during pyrolysis.

Previous studies showed that the pyrolysis temperature has an important influence on the catalytic activity of Fe−N/C catalysts,[9] since calcination at a low temperature may facilitate the incorporation of nitrogen and iron into the carbon matrix while a high pyrolysis temperature can increase the electrical conductivity of the carbon material. To find an optimum pyrolysis temperature for our self-supporting Fe−N/C catalyst, the Fe−bidppz precursor was pyrolyzed at various temperatures (700−900 °C). The X-ray diffraction (XRD) patterns shown in Figure S1a (Supporting Information) display the structures of the catalysts prepared at different temperatures. It is clearly seen that the peak around 25° becomes stronger and narrower with increasing temperature, indicating that a higher pyrolysis temperature may lead to more ordered graphitic carbon. Figure S1b compares the Raman spectra of Fe−N/C catalysts synthesized at different pyrolysis temperatures. The ratios of the D band to G band integrated intensities (I_D/I_G) are 3.38 (700 °C), 3.13 (750 °C), 2.87 (800 °C), 2.44 (850 °C), and 1.78 (900 °C). As the highly ordered graphite shows a very weak D-band, the decreasing value of I_D/I_G with increasing temperature proves the formation of more and more ordered graphitic structure domains during heat treatment.[35] A more ordered structure with graphitic structure domains is beneficial for increasing the electrical conductivity of the derived carbon. The elemental compositions of Fe−N/C samples were determined by X-ray photoelectron spectroscopy (XPS) (Table S1, Supporting Information). The content of carbon increases with the pyrolysis temperature, while the contents of nitrogen and iron are reduced due to high temperatures. The content of iron decreases sharply from 0.51 to 0.28 atom % when the pyrolysis temperature increases from 750 to 800 °C, indicating the higher the pyrolysis temperature, the greater the degree of agglomeration. Electrochemical measurements (Figure S2, Supporting Information) confirm that the catalyst with the best ORR activity is the one obtained by pyrolyzing Fe−bidppz at 800 °C (Fe−N/C-800) in both alkaline and acidic conditions, implying that the catalyst obtained at 800 °C has optimal comprehensive conditions considering the effective factors, including the content of nitrogen and iron and the structure and electrical conductivity of carbon.

The scanning electron microscopy (SEM) image of the Fe−bidppz precursor (Figure 2a) shows that the precursor has an elongated sheetlike morphology and the precursor sheets broke into small pieces during pyrolysis at 800 °C (Figure 2b,c). The Brunauer−Emmet−Teller (BET) surface areas of Fe−bidppz and Fe−N/C-800 are 77 and 56 $m^2\ g^{-1}$, respectively (Figure S3a,b, Supporting Information). This decrease of surface area may be attributed to the collapsing of pores in the Fe−bidppz porous network. The Barrett−Joyner−Halenda (BJH) analysis indicates that the Fe−N/C-800 catalyst contains mesopores ~3.9 and 6.6 nm in diameter (Figure S3c). It is most likely that these mesopores are helpful for the ORR activity of Fe−N/C-800 catalyst. The transmission electron microscopy (TEM)

dx.doi.org/10.1021/ja504696r | J. Am. Chem. Soc. 2014, 136, 11027−11033

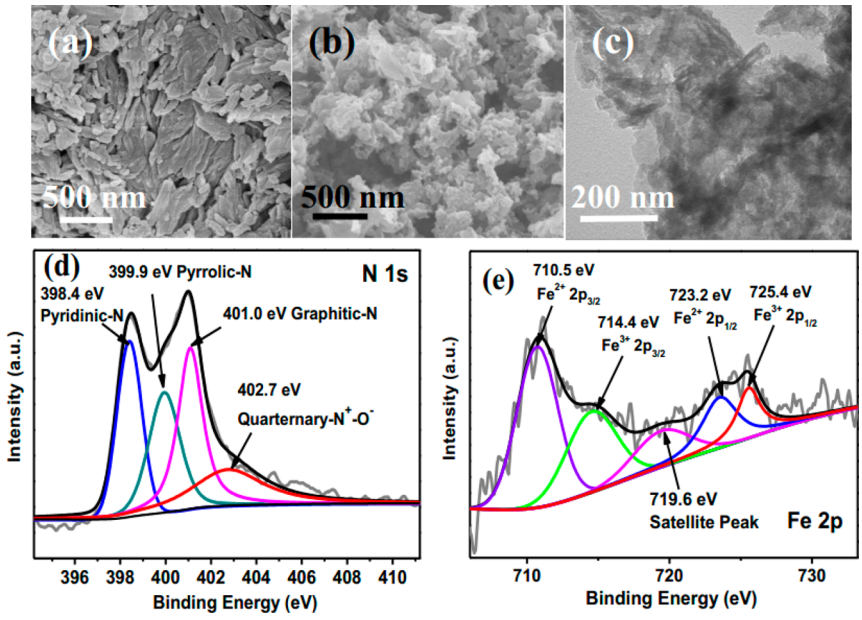

Figure 2. SEM image of the Fe−bidppz precursor (a). SEM image (b) and TEM image (c) of the Fe−N/C-800 catalyst. N 1s XPS spectrum (d) and Fe 2p XPS spectrum (e) of the Fe−N/C-800 catalyst.

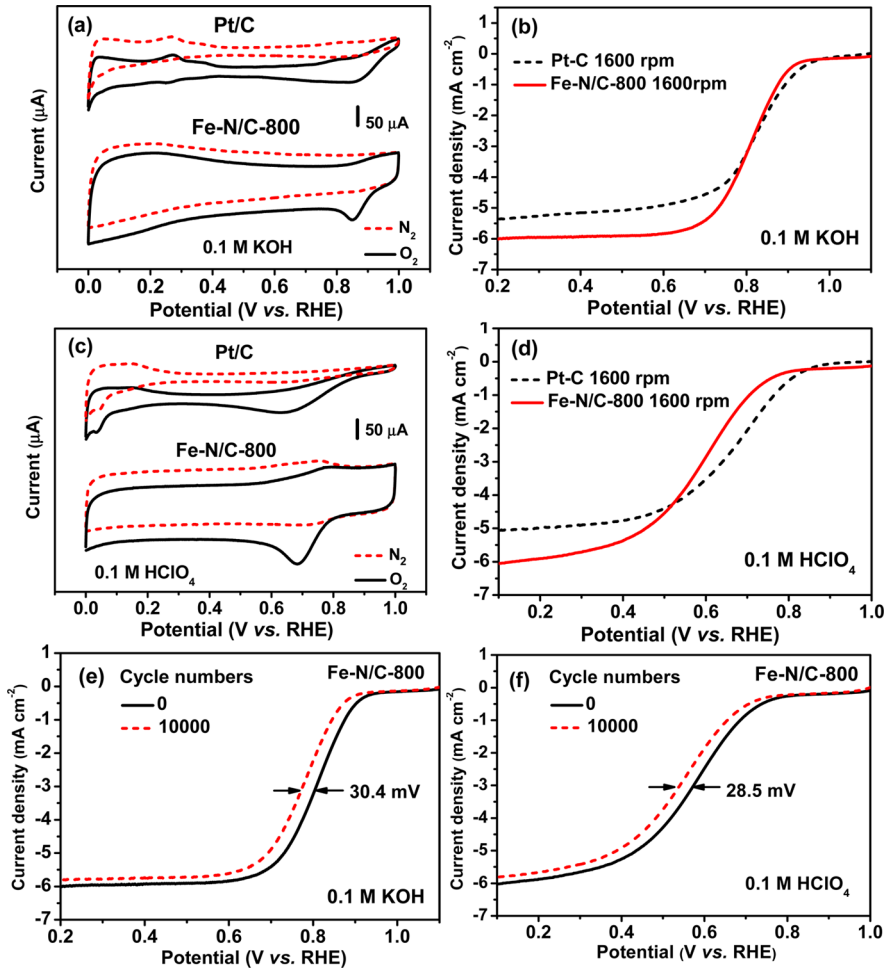

Figure 3. Cyclic voltammograms (a) and RDE voltammograms (b) of Pt/C and Fe−N/C-800 in O_2-saturated 0.1 M KOH. Cyclic voltammograms (c) and RDE voltammograms (d) of Pt/C and Fe−N/C-800 in O_2-saturated 0.1 M $HClO_4$. Endurance test of the Fe−N/C-800 catalyst for 10 000 cycles in O_2-saturated 0.1 M KOH (e) and 0.1 M $HClO_4$ (f). For all tests, the catalyst loading is 0.1 mg cm^{-2} and the scan rate is 10 mV s^{-1}.

dx.doi.org/10.1021/ja504696r | J. Am. Chem. Soc. 2014, 136, 11027−11033

image (Figure 2c) and XRD pattern of Fe−N/C-800 (Figure S1a, Supporting Information) reveal that no iron particles can be found in the Fe−N/C-800 sample, indicating that the acid leaching process removes most of the inactive iron particles since the XRD pattern and TEM image of the pyrolyzed product before acid leaching show the existence of iron particles (Figure S4, Supporting Information). Electrochemical measurements show the leaching process is significant to the ORR activity of the catalyst. From Figure S5 (Supporting Information), it can be seen that the catalytic activity of Fe−N/C-800 is greatly enhanced after acid leaching because the bulk iron particles formed during pyrolysis are inactive and block the surface active sites.

XPS spectra reveal the elemental information on the Fe−N/C-800 catalyst. From the survey scan of Fe−N/C-800 shown in Figure S6 (Supporting Information), it can be seen that the Fe−N/C-800 catalyst contains four kinds of elements, carbon (87.25%), nitrogen (9.62%), oxygen (2.85%), and iron (0.28%). The N 1s spectrum (Figure 2d) can be divided into several peaks at 398.4, 399.1, 399.9, 401.0, and 402.7 eV, which can be assigned to pyridinic N (24.73%), pyrrolic N (24.23%), graphitic N (30.27%), and quarternary N^+-O^- (20.77%) on the basis of the respective binding energies.[36,37] The graphitic N was reported to play a crucial role in oxygen reduction;[38] besides, pyridinic N and pyrrolic N can serve as metal-coordination sites due to their lone-pair electrons. These three kinds of ORR active nitrogen are of high content in our Fe−N/C-800 elecrocatalyst, which leads to a high catalytic activity. Figure 2e shows the Fe 2p spectrum. According to previous reports,[39,40] the peaks at 710.5 and 714.4 eV can be assigned to the binding energies of the $2p_{3/2}$ orbitals of Fe^{2+} and Fe^{3+} species, respectively. For the $2p_{1/2}$ band, the peak at 723.2 eV is attributed to the binding energy of Fe^{2+}, and the peak for Fe^{3+} is observed at 725.4 eV. The peak at 719.6 eV is a satellite peak. The XPS survey scan suggests a trace amount of S as well, which is likely to be present in the form of S−C and SO_x.[41] A control experiment shows that the trace amount of S has no obvious contribution to the high activity of our catalyst (details in the Supporting Information, Figure S7).

To examine the electrocatalytic activity of the Fe−N/C-800 catalyst, cyclic voltammetry (CV) measurements were carried out for Pt/C and Fe−N/C-800 catalysts in O_2- or N_2-saturated 0.1 M KOH (Figure 3a) and 0.1 M $HClO_4$ (Figure 3c) at the same catalyst loading of 0.1 mg cm^{-2}, and the Pt loading for the Pt/C catalyst was 20 μg cm^{-2}. In an alkaline electrolyte, Fe−N/C-800 shows a quasi-rectangular double-layer capacity current in N_2,[42] and a well-defined ORR peak in O_2 with a peak potential of 851 mV is observed, which is a little negative compared to that of Pt/C (868 mV). However, the ORR peak current of Fe−N/C-800 is 90.2 μA, much higher than that of Pt/C (60.8 μA). In an acidic electrolyte, Fe−N/C-800 displays a pair of symmetric peaks at about 750 mV, which indicates a redox reaction occurs between Fe(II) and Fe(III) during this process. A small oxidation peak also appears at 780 mV in saturated O_2 for Fe−N/C-800 in acidic solution, indicating iron doping in the carbon material may play the role of a mediator in the electron-transfer processes during the oxygen reduction reaction occurring in acidic conditions. A previous study[43] proposed an oxygen reduction mechanism for $CoFeN_x$/C in an acidic electrolyte in which transition-metal ions can act as a mediator in the electron-transfer process. The ORR peak potential for Fe−N/C-800 in an acid is 687 mV, which is slightly more positive than that for Pt/C (672 mV). More importantly, the ORR peak current in 0.1 M $HClO_4$ for Fe−N/C-800 is much larger than that in 0.1 M KOH, reaching 124.2 μA, while the peak current of Pt/C in an acid is only 65.0 μA. The higher capacitance currents of Fe−N/C-800 in CV suggest that Fe−N/C-800 promotes O_2 transport within the catalyst layer due to the mesopores in the Fe−N/C-800 catalyst.[44] Similar performances of the ORR activities of Pt/C and Fe−N/C-800 catalysts were observed by rotating disk electrode (RDE) experiments at 1600 rpm and 10 mV s^{-1}. Figure 3b shows that the onset potential for the Fe−N/C-800 catalyst in alkaline conditions (923 mV) is ∼33 mV lower than that of Pt/C (956 mV) and the half-wave potentials ($E_{1/2}$) for Fe−N/C-800 and Pt/C are 809 and 818 mV, respectively. The polarization curves performed in acidic conditions are displayed in Figure 3d. It can be seen that the value of the onset potential and the half-wave potential on an Fe−N/C-800 catalyst electrode are only 38 mV and 59 mV more negative than those for Pt/C. The limiting current densities (j_L) of Fe−N/C-800 are 6.06 and 6.09 mA cm^{-2} in KOH and $HClO_4$ at a rotating speed of 1600 rpm, respectively, which are close to the theoretical value determined by the Koutecky−Levich equation. These electrochemical values are close to those of the previously reported active ORR catalysts; thus, our Fe−N/C-800 catalyst has a high ORR activity not only in an alkaline electrolyte but also in an acidic electrolyte. The modest specific surface area (56 m^2 g^{-1}) and the high ORR activity of Fe−N/C-800 comparable to those of other kinds of M−N/C catalysts with specific surface areas as high as hundreds of square meters per gram imply that our Fe−N/C-800 catalyst may have a much higher density of surface active sites than previously reported M−N/C catalysts.[10,22,41]

Because of iron doping in the Fe−N/C-800 catalyst, there is a question of whether iron species serve as the active site. Previous works have proposed two different hypotheses to describe the active sites in the M−N/C ORR catalyst. One is the $M-N_x$ species,[44,45] and the other is the N atoms doping the carbon matrix.[46] The latter is the same as the nonmetal N/C catalyst.[4,47] The ORR activity of Fe−N/C-800 is most probably considered to follow the former hypothesis that the $Fe-N_x$ may act as the major active sites. A control experiment by pyrolyzing the pure bidppz was conducted to confirm the viewpoint that $Fe-N_x$ plays a key role in the high catalytic activity of Fe−N/C-800. The pyrolyzed pure bidppz catalyst has a N content (10.15%) higher than that of the Fe−N/C-800 catalyst (Table S2, Supporting Information), while the ORR activities of the pyrolyzed pure bidppz catalyst are much poorer than those of the Fe−N/C-800 catalyst in both electrolytes, especially in acidic conditions (Figure S7c,d, Supporting Information). Although the $Fe-N_x$ active sites need to be further confirmed by other characterization methods, the obvious improvement of ORR activity by introduction of iron suggests that the $Fe-N_x$ species make a major contribution to the activity of Fe−N/C-800. Particularly, according to the peak area of Fe^{2+} and Fe^{3+} from the Fe 2p XPS spectrum, it is found that the use of Fe^{2+} as the iron precursor results in a quite high percentage of Fe^{2+} in our Fe−N/C-800 catalyst. Since $Fe^{2+}-N_4$ can serve as the active sites according to a previous work,[44] abundant Fe^{2+} species may play a major role in superior ORR activity of the Fe−N/C-800 catalyst.

Although some reported NPMCs exhibit relatively high ORR activities, durability is of significance for practical applications. Cycling durability tests in O_2-saturated electrolytes were carried out to test the stability of Fe−N/C-800 for 10 000 cycles. The

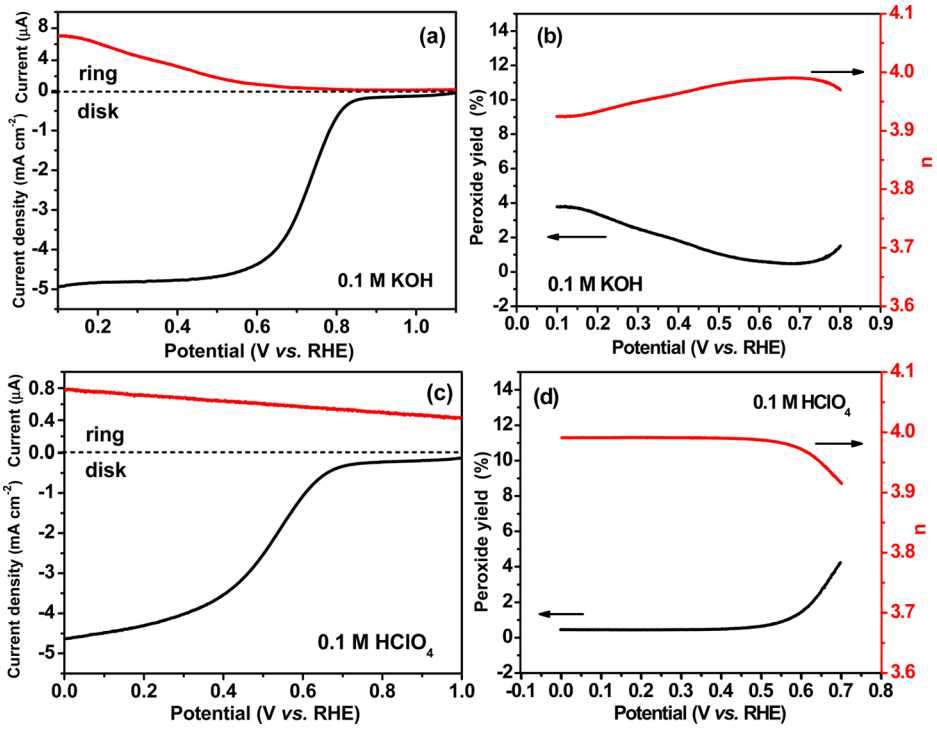

Figure 4. RRDE voltammograms (a) and peroxide yield (black) with regard to the total oxygen reduction products and the electron-transfer number (n) (red) (b) of Fe−N/C-800 in O_2-saturated 0.1 M KOH. RRDE voltammograms (c) and peroxide yield (black) with regard to the total oxygen reduction products and n (red) (d) of Fe−N/C-800 in O_2-saturated 0.1 M $HClO_4$. For all tests, the catalyst loading is 0.1 mg cm^{-2}, the rotating speed is 900 rpm, and the scan rate is 10 mV s^{-1}.

polarization curves recorded after 10 000 cycles show a negative shift of $E_{1/2}$ of 30.4 and 28.5 mV in alkaline and acidic electrolytes (Figure 3e,f), respectively, indicating its durability is superior to that of Pt/C (Figure S8, Supporting Information). The obvious inactivation behavior of Pt/C (large negative shifts of onset potential and $E_{1/2}$, but no obvious decrease in j_L) is mainly ascribed to the dissolution of Pt nanoparticles at high potentials.[48] Different from Pt/C, the simultaneous decrease in $E_{1/2}$ and j_L of Fe−N/C-800 is attributed to the oxidation of the carbon support as well as the oxidation of active sites, as active site oxidation will only lead to a negative shift of the onset potential and $E_{1/2}$.[43] The limiting currents only decrease by 5% and 6.3% after 10 000 cycles in 0.1 M KOH and $HClO_4$, respectively, implying that the self-supporting carbon in our catalyst is a good candidate for the carbon support. It is worth noting that our Fe−N/C-800 catalyst shows superior ORR activity and high stability in an acidic electrolyte, proving that the Fe−N_x sites in the Fe−N/C-800 catalyst are quite stable in an acidic environment. Notably, the Fe−N/C-800 catalyst shows better tolerance toward methanol than Pt/C. As shown in Figure S9 (Supporting Information), a small decrease of the ORR peak is observed for Fe−N/C-800, indicating little influence of methanol on the ORR activity of our Fe−N/C-800 catalyst. In contrast, the ORR peaks of Pt/C disappear and methanol oxidation peaks appear because the electro-oxidation of methanol hinders the ORR process. These results indicate that the Fe−N/C-800 catalyst is superior to Pt/C as an ORR catalyst for direct methanol fuel cells.

ORR polarization curves of the Fe−N/C-800 catalyst at different rotation rates from 400 to 1600 rpm were measured to determine whether the ORR of Fe−N/C-800 occurs by four-electron (4e) reduction of oxygen to produce H_2O. Generally, the 4e process is believed to be more efficient than the 2e process that produces H_2O_2, in addition, H_2O_2 formed during the 2e process is poisonous to catalysts. ORR polarization curves of Fe−N/C-800 at rotation rates from 400 to 1600 rpm are shown in Figure S10a,c (Supporting Information). On the basis of the Koutecky−Levich equation,[10] four J^{-1} versus $\omega^{-1/2}$ plots were obtained (Figure S10b,d). Good linear relationships between J^{-1} and $\omega^{-1/2}$ are observed, indicating first-order reaction kinetics with respect to the O_2 concentration. We calculated the electron-transfer number (n) from the slope of each line. For an alkaline electrolyte, the average value is 4.15, while the calculated value is 4.09 for an acidic electrolyte. Therefore, the oxygen reduction reaction on the Fe−N/C-800 catalyst in both electrolytes follows the four-electron-transfer pathway, corresponding to the complete reduction of oxygen into water. To further validate this conclusion, rotating ring−disk electrode (RRDE) measurements were performed to determine the four-electron selectivity of the Fe−N/C-800 catalyst. Parts a and c of Figure 4 show the disk and ring currents measured at 900 rpm in 0.1 M KOH and 0.1 M $HClO_4$, respectively. The onset potential for H_2O_2 generation in 0.1 M KOH is lower than the onset potential of ORR, which is similar to the behavior of Pt catalysts.[49] The behavior of the ring current curve in 0.1 M $HClO_4$ is different from that in 0.1 M KOH, and the ring current in acidic conditions is about 10 times smaller than that in alkaline conditions under low potentials. The hydrogen peroxide yield (%) and the electron-transfer number (n) curves (Figure 4b,d) can be directly calculated from the disk currents (i_d) and the ring currents (i_r). As shown in Figure 4b, the peroxide species yield in alkaline solution is less than 4% in the measured potential range from 1.1 to 0.1 V and the average n is ~3.96. For an acidic electrolyte, Figure 4d shows that the value of n is almost constant at 4.00 from 0 to 0.5 V and gradually decreases to

dx.doi.org/10.1021/ja504696r | J. Am. Chem. Soc. 2014, 136, 11027−11033

~3.92 at potentials higher than 0.5 V. The average n obtained from the curve is ~3.99, which is slightly larger than that in KOH. The electron-transfer number calculated from RRDE measurements is in agreement with the electron-transfer number based on the Koutecky–Levich plots, signaling mainly the 4e pathway for the Fe–N/C-800-catalyzed ORR process. Previous studies have demonstrated that the higher overpotential for ORR in acidic electrolytes is due to the hydrogen peroxide intermediate (H_2O_2) in acidic media being less stable on Fe^{2+}–N/C active sites than the Lewis basic form (HO_2^-) in alkaline media. The destabilization of H_2O_2 on Fe^{2+}–N/C active sites in an acid results in the requirement of a secondary active site to reduce or disproportionate H_2O_2. The high surface active site density of the Fe–N/C-800 catalyst will facilitate this process because of the high probability for H_2O_2 to be adsorbed by a secondary active site immediately, leading to an onset potential only 38 mV negative of that for Pt/C and an electron-transfer number as high as 3.99 in acidic media.

CONCLUSIONS

In this work, we have developed a highly efficient self-supporting M–N/C ORR electrocatalyst in both alkaline and acidic conditions by pyrolysis of a complex precursor, Fe–bidppz, in argon. The pyrolysis temperature largely affects the ORR activity, and the optimal catalyst pyrolyzed at 800 °C exhibits the highest ORR activity comparable to that of commercial Pt/C. Although the specific surface area of Fe–N/C-800 is not high, the activity of the Fe–N/C-800 catalyst is comparable to that of the Pt/C catalyst in both alkaline and acidic media, indicating a high active site density of our Fe–N/C-800 catalyst. We propose that the major active sites in the Fe–N/C-800 catalyst are the N-binding iron species (Fe–N_x), as the introduction of iron into the catalyst greatly enhances the ORR activity. Moreover, the Fe–N/C-800 catalyst shows better stability and tolerance of methanol than the commercial Pt/C catalyst. There is a very small decrease of the limiting current after 10 000 cycles, demonstrating that the self-supporting carbon in the Fe–N/C-800 catalyst is a good candidate for the carbon support. More notably, the oxygen reduction reaction on the Fe–N/C-800 catalyst in alkaline and acidic media follows the efficient four-electron-transfer pathway, indicating the complete reduction of oxygen into water. Taken together, our developed self-supporting Fe–N/C-800 catalyst could find potential applications in PEMFCs with superior ORR performance and high stability.

ASSOCIATED CONTENT

Supporting Information

Experimental details, XRD patterns, Raman spectra, elemental compositions from XPS, nitrogen adsorption/desorption isotherms, and supporting electrochemical analysis. This material is available free of charge via the Internet at http://pubs.acs.org.

AUTHOR INFORMATION

Corresponding Author

anwuxu@ustc.edu.cn

Notes

The authors declare no competing financial interest.

ACKNOWLEDGMENTS

Support from the National Basic Research Program of China (Grants 2011CB933700 and 2010CB934700) and the National Natural Science Foundation of China (Grant 21271165) is gratefully acknowledged.

REFERENCES

(1) Wu, J. B.; Yang, H. *Acc. Chem. Res.* **2013**, *46*, 1848–1857.
(2) Chen, T.; Cai, Z.; Yang, Z.; Li, L.; Sun, X.; Huang, T.; Yu, A.; Kia, H. G.; Peng, H. *Adv. Mater.* **2011**, *23*, 4620–4625.
(3) Zheng, Y.; Jiao, Y.; Chen, J.; Liu, J.; Liang, J.; Du, A.; Zhang, W.; Zhu, Z.; Smith, S. C.; Jaroniec, M.; Lu, G. Q.; Qiao, S. Z. *J. Am. Chem. Soc.* **2011**, *133*, 20116–20119.
(4) Deng, D.; Pan, X.; Yu, L.; Cui, Y.; Jiang, Y.; Qi, J.; Li, W.-X.; Fu, Q.; Ma, X.; Xue, Q.; Sun, G.; Bao, X. *Chem. Mater.* **2011**, *23*, 1188–1193.
(5) Su, H.-Y.; Gorlin, Y.; Man, I. C.; Calle-Vallejo, F.; Nørskov, J. K.; Jaramillo, T. F.; Rossmeisl, J. R. *Phys. Chem. Chem. Phys.* **2012**, *14*, 14010–14022.
(6) Esposito, D. V.; Chen, J. G. *Energy Environ. Sci.* **2011**, *4*, 3900–3912.
(7) Carver, C. T.; Matson, B. D.; Mayer, J. M. *J. Am. Chem. Soc.* **2012**, *134*, 5444–5447.
(8) Samanta, S.; Sengupta, K.; Mittra, K.; Bandyopadhyay, S.; Dey, A. *Chem. Commun.* **2012**, *48*, 7631–7633.
(9) Zhao, Y.; Watanabe, K.; Hashimoto, K. *J. Am. Chem. Soc.* **2012**, *134*, 19528–19531.
(10) Peng, H.; Mo, Z.; Liao, S.; Liang, H.; Yang, L.; Luo, F.; Song, H.; Zhong, Y.; Zhang, B. *Sci. Rep.* **2013**, *3*, 1765.
(11) Chung, H. T.; Won, J. H.; Zelenay, P. *Nat. Commun.* **2013**, *4*, 1922.
(12) Chen, Z.; Higgins, D.; Yu, A.; Zhang, L.; Zhang, J. *Energy Environ. Sci.* **2011**, *4*, 3167–3192.
(13) Jaouen, F.; Proietti, E.; Lefevre, M.; Chenitz, R.; Dodelet, J. P.; Wu, G.; Chung, H. T.; Johnston, C. M.; Zelenay, P. *Energy Environ. Sci.* **2011**, *4*, 114–130.
(14) Oberst, J. L.; Thorum, M. S.; Gewirth, A. A. *J. Phys. Chem. C* **2012**, *116*, 25257–25261.
(15) Herranz, J.; Jaouen, F.; Lefevre, M.; Kramm, U. I.; Proietti, E.; Dodelet, J.-P.; Bogdanoff, P.; Fiechter, S.; Abs-Wurmbach, I.; Bertrand, P.; Arruda, T.; Mukerjee, S. *J. Phys. Chem. C* **2011**, *115*, 16087–16097.
(16) Jasinski, R. *Nature* **1964**, *201*, 1212–1213.
(17) Wiesener, K. *Electrochim. Acta* **1986**, *31*, 1073–1078.
(18) van Veen, J. A. R.; Colijn, H. A.; van Baar, J. F. *Electrochim. Acta* **1988**, *33*, 801–804.
(19) Bezerra, C. W. B.; Zhang, L.; Lee, K. C.; Liu, H. S.; Marques, A. L. B.; Marques, E. P.; Wang, H. J.; Zhang, J. J. *Electrochim. Acta* **2008**, *53*, 4937–4951.
(20) Gupta, S.; Tryk, D.; Bae, I.; Aldred, W.; Yeager, E. *J. Appl. Electrochem.* **1989**, *19*, 19–27.
(21) Bashyam, R.; Zelenay, P. *Nature* **2006**, *443*, 63–66.
(22) Wu, G.; More, K. L.; Johnston, C. M.; Zelenay, P. *Science* **2011**, *332*, 443–447.
(23) Choi, J.; Hsu, R.; Chen, Z. *J. Phys. Chem. C* **2010**, *114*, 8048–8053.
(24) Chung, H. T.; Johnston, C. M.; Zelenay, P. *ECS Trans.* **2009**, *24*, 485–492.
(25) Lefevre, M.; Proietti, E.; Jaouen, F.; Dodelet, J. P. *Science* **2009**, *324*, 71–74.
(26) Wu, G.; Chen, Z.; Artyushkova, K.; Garzon, F. H.; Zelenay, P. *ECS Trans.* **2008**, *16*, 159–170.
(27) Ferrandon, M.; Kropf, A. J.; Myers, D. J.; Artyushkova, K.; Kramm, U.; Bogdanoff, P.; Wu, G.; Johnston, C. M.; Zelenay, P. *J. Phys. Chem. C* **2012**, *116*, 16001–16013.
(28) Wu, G.; Johnston, C. M.; Mack, N. H.; Artyushkova, K.; Ferrandon, M.; Nelson, M.; Lezama-Pacheco, J. S.; Conradson, S. D.; More, K. L.; Myers, D. J.; Zelenay, P. *J. Mater. Chem.* **2011**, *21*, 11392–11405.

(29) Yuan, X.; Zeng, X.; Zhang, H.-J.; Ma, Z.-F.; Wang, C.-Y. *J. Am. Chem. Soc.* **2010**, *132*, 1754−1755.
(30) Chen, X.-M.; Tong, M.-L. *Acc. Chem. Res.* **2007**, *40*, 162−170.
(31) Zhu, Q.; Peng, Y.; Lin, L.; Fan, C.-M.; Gao, G.-Q.; Wang, R.-X.; Xu, A.-W. *J. Mater. Chem. A* **2014**, *2*, 4429−4437.
(32) Johns, I. B.; McElhill, E. A.; Smith, J. O. *Ind. Eng. Chem. Prod. Res. Dev.* **1962**, *1*, 2−6.
(33) Yang, X.; Li, Z.; Zhi, J.; Ma, J.; Hu, A. *Langmuir* **2010**, *26*, 11244−11248.
(34) Kim, T.-W.; Park, I.-S.; Ryoo, R. *Angew. Chem., Int. Ed.* **2003**, *42*, 4375−4379.
(35) Sadezky, A.; Muckenhuber, H.; Grothe, H.; Niessner, R.; Pöschl, U. *Carbon* **2005**, *43*, 1731−1742.
(36) Zhang, Y.; Ge, J.; Wang, L.; Wang, D.; Ding, F.; Tao, X.; Chen, W. *Sci. Rep.* **2013**, *3*, 2771.
(37) Shin, D.; Jeong, B.; Mun, B. S.; Jeon, H.; Shin, H.-J.; Baik, J.; Lee, J. *J. Phys. Chem. C* **2013**, *117*, 11619−11624.
(38) Liu, R.; Wu, D.; Feng, X.; Müllen, K. *Angew. Chem., Int. Ed.* **2010**, *49*, 2565−2569.
(39) Gupta, A.; Kumar, A.; Waghmare, U. V.; Hegde, M. S. *Chem. Mater.* **2009**, *21*, 4880−4891.
(40) Kong, H.; Song, J.; Jang, J. *Chem. Commun.* **2010**, *46*, 6735−6737.
(41) Chang, Y. Q.; Hong, F.; He, C. X.; Zhang, Q. L.; Liu, J. H. *Adv. Mater.* **2013**, *25*, 4794−4799.
(42) Yang, S. B.; Zhi, L. J.; Tang, K.; Feng, X. L.; Maier, J.; Müllen, K. *Adv. Funct. Mater.* **2012**, *22*, 3634−3640.
(43) Jiang, R.; Chu, D. *J. Power Sources* **2014**, *245*, 352−361.
(44) Ramaswamy, N.; Tylus, U.; Jia, Q.; Mukerjee, S. *J. Am. Chem. Soc.* **2010**, *135*, 15443−15449.
(45) Lefevre, M.; Dodelet, J. P.; Bertrand, P. *J. Phys. Chem. B* **2002**, *106*, 8705−8713.
(46) Nabae, Y.; Moriya, S.; Matsubayashi, K.; Lyth, S. M.; Malon, M.; Wu, L.; Islam, N. M.; Koshigoe, Y.; Kuroki, S.; Kakimoto, M.-a.; Miyata, S.; Ozaki, J.-i. *Carbon* **2010**, *48*, 2613−2624.
(47) Silva, R.; Voiry, D.; Chhowalla, M.; Asefa, T. *J. Am. Chem. Soc.* **2013**, *135*, 7823−7826.
(48) Borup, R.; Meyers, J.; Pivovar, B.; Kim, Y. S.; Mukundan, R.; Garland, N.; Myers, D.; Wilson, M.; Garzon, F.; Wood, D.; Zelenay, P.; More, K.; Stroh, K.; Zawodzinski, T.; Boncella, J.; McGrath, J. E.; Inaba, M.; Miyatake, K.; Hori, M.; Ota, K.; Ogumi, Z.; Miyata, S.; Nishikata, A.; Siroma, Z.; Uchimoto, Y.; Yasuda, K.; Kimijima, K.; Iwashita, N. *Chem. Rev.* **2007**, *107*, 3904−3951.
(49) Schmidt, T. J.; Stamenkovic, V.; Arenz, M.; Markovic, N. M.; Ross, P. N., Jr. *Electrochim. Acta* **2002**, *47*, 3765−3776.